

# Computational Design Optimization of a Smart Material Shape Changing Building Skin Tile

Robert J. Zupan<sup>1</sup>, Jing Xu<sup>2</sup>, Richard V. Beblo<sup>3</sup>, Dale T. Clifford<sup>4</sup>, Ankush Aggarwal<sup>5</sup>, and John C. Brigham<sup>6</sup>

<sup>1</sup>PhD, Post-Doctoral Fellow, Dept. of Civil and Environmental Engineering, Univ. of Pittsburgh,  
Email: rjz6@pitt.edu (corresponding author)

<sup>2</sup>PhD Student, Dept. of Civil and Environmental Engineering, Univ. of Pittsburgh, Email:  
jix57@pitt.edu

<sup>3</sup>PhD, Research Engineer, University of Dayton Research Institute, Email:  
richard.beblo.1@us.af.mil

<sup>4</sup>PhD, Associate Professor, College of Architecture and Environmental Design, California  
Polytechnic State Univ., Email: dtcliffo@calpoly.edu

<sup>5</sup>PhD, Lecturer, School of Engineering, Univ. of Glasgow, Email:  
Ankush.Aggarwal@glasgow.ac.uk

<sup>6</sup>PhD, Professor, Dept. of Engineering, Durham Univ., Email: john.brigham@durham.ac.uk

## ABSTRACT

The development and evaluation of a computational approach for optimal design of a smart material shape changing building skin is presented and numerically evaluated. Specifically, a unique shape-based approach is utilized to create an optimization approach to identify the activation and actuation mechanisms to minimize the difference between a desired shape and the estimated morphed shape. Three potential metrics of shape difference are considered and their capability to facilitate an efficient optimization process leading to accurate shape matching is evaluated. Details of the optimal design framework are presented, particularly focusing on the shape difference

24 metrics as well as the strategy to parameterize the activation of the smart material. In particular, the  
25 parameterization strategy is a unique approach to easily integrate controllable localized activation  
26 within a smart material structure in a generally applicable way that does not limit the design search  
27 space. A series of numerical design examples are presented based on the concept of a smart  
28 material (e.g., shape memory polymer) shape changing tile that can be activated and actuated in  
29 a variety of ways to achieve desirable surface wrinkle patterns. These numerical design examples  
30 are applied to both 2D and 3D problems and consider a variety of parameterizations and target  
31 shapes. Results indicate that the shape-based approach can consistently determine the mechanisms  
32 of morphing needed to accurately match a target shape. Furthermore, it is shown that localized  
33 material activation can lead to not only a more accurate shape but also requires less energy and  
34 actuation devices to do so.

35 **Keywords:** Self-shading, Smart Material, Optimization, Objective Function, Hausdorff, Com-  
36 putational Mechanics

## 37 INTRODUCTION

38 Responsive building skins have been shown to have effects on all the main energy consumers  
39 of commercial buildings: lighting, ventilation, and heating and cooling (Shameri et al. 2011).  
40 Examples include the skin used on the Media-TIC building (Dewidar et al. 2013), which uses a  
41 light sensor to measure thermal loads on a building and inflates portions of the skin in order to  
42 increase insulation during times of high thermal loading, and the Heliotrace system (Dewidar et al.  
43 2013) and the responsive skin of the Al Bahar towers (Cilento 2012), which both utilize a series of  
44 mechanical apertures that open or close portions of the skin, allowing different amounts of light to  
45 enter the building. In most cases the current technologies are binary, either activated or inactivated  
46 based on a stimulus threshold, or have a limited number of configurations. Thus, significant work  
47 still remains to achieve technologies that can adapt to multiple environmental states and have a  
48 higher level of customization. One possibility proposed to increase functionality of responsive  
49 building façade is the integration of smart materials (Jani et al. 2014; Mather et al. 2009; Lampert  
50 2004; Otsuka and Wayman 1999).

51 The technologies being developed for shape changing building skins that use smart materials  
52 have primarily relied upon passive mechanisms, in that the shape change that occurs is caused  
53 by the material being activated by changes in the surrounding environmental conditions (e.g.,  
54 moisture change (Holstov et al. 2015) or temperature change (Barrett and Barrett 2016)). Passive  
55 use of the smart material has the benefit of not requiring any additional intervention or energy  
56 costs to the user beyond maintenance requirements. Yet, passive use of the material may limit  
57 the extent that the behavior of the structure can be customized and may limit feasibility of certain  
58 applications or material types if the activating environmental condition does not correlate with the  
59 desired material change. Alternatively, active use of smart materials for shape changing structures  
60 that include a mechanism to apply activation energy and/or actuation to the structure have the  
61 obvious disadvantage of energy consumption, but can substantially increase the range of potential  
62 shape changes and the potential applications of the technology overall. There have been several  
63 application areas of smart material structures where this benefit of active use has outweighed the  
64 additional energy costs, such as morphing aircraft applications (Liu et al. 2014; Yu et al. 2009; Sun  
65 et al. 2015). Although active use of smart materials for shape changing structures can significantly  
66 expand the potential functions of the structure, this expansion can also substantially increase the  
67 initial challenge of designing the smart material structure.

68 With any degree of complexity in the desired behavior, the active use of smart materials for  
69 shape changing structures can include nearly infinite non-trivial potential design solutions, when  
70 potentially seeking to define localized stimulation/activation, a multitude of mechanical actuation  
71 methods, or even the use of multiple smart materials together. Such design problems are often  
72 best handled through a computational optimal design approach, which have already been used for  
73 several smart material structure design applications (Molinari et al. 2015; Woods and Friswell 2016;  
74 Liu et al. 2014; Yu et al. 2009; Sun et al. 2015; Lu and Kota 2003; Prock et al. 2002; Namgoong  
75 et al. 2006; Mohaghegh Motlagh 2014; Wang and Brigham 2012). Computational approaches are  
76 particularly beneficial for problems that have non-trivial and/or non-intuitive solutions, and complex  
77 objectives and constraints. Although substantial work has been done developing computational

78 design methods for various applications, with any new application there are new and unique  
79 challenges, ranging from the definition of the forward model and its parameterization to the  
80 quantification of the design objective and constraints.

81 The current study presents a computational framework for the design of the active mechanisms  
82 for a smart material building skin tile to optimally achieve a desired shape change. The target of  
83 shape change is chosen as it aligns with the prior work using hygromorphic structures (Bridgens  
84 2018), which was noted to be largely for aesthetic reasons thus far, while also allowing for inclusion  
85 of other more functional objectives, such as increasing shading similar to the work in (Barrett  
86 and Barrett 2016). In other words, it is assumed that some prior analysis to define the desired  
87 combination of appearance and function has been performed to provide the target shape change to  
88 be designed toward. As such, one particular focus of the study is on determining an appropriate  
89 objective function for the design approach that quantifies the difference between the desired shape  
90 change and the shape change predicted by the forward model for the optimization procedure. In  
91 addition, focus is also placed on the strategy to define the unknown design parameters, particularly  
92 to ensure the localized activation is feasible to implement without sacrificing the shape change  
93 capability. Although more generally applicable, the design strategy is presented in the context of  
94 an example design of the mechanical actuation and material activation of tile entirely comprised of  
95 a homogeneous smart material. In the following section, the details of this exemplar smart material  
96 shape changing building skin tile are provided. In Section 3 the general computational inverse  
97 problem for the design of a smart material building skin tile is presented. Numerical examples,  
98 their results, and discussion are then given in Section 4, which is followed by concluding remarks  
99 in Section 5.

## 100 DESIGN CONCEPT

101 The design concept considered herein is an adaptive shape changing “wrinkled” surface tile  
102 based upon the prior work developing building surface “cactus tiles” by Clifford (Clifford 2019). The  
103 original cactus tile objective was to have static “wrinkled” surface tiles that were both aesthetically  
104 pleasing and had functional benefits in terms of self-shading. However, it is envisioned that adding

105 the capability of such tiles to change between wrinkle patterns, would further enhance the original  
 106 benefits and potentially include many other functional behaviors (Clifford 2019; Zupan et al. 2017;  
 107 Zupan et al. 2018). As shown in Figure 1, the proposed mechanism to produce a tile that can morph  
 108 between different wrinkle patterns (i.e., shape changing cactus tile) is envisioned to be controllable  
 109 activation of the smart material comprising the tile (e.g., softening) and mechanical actuation to  
 110 deform the tile into a desired shape. For the sake of simplicity, this work does not consider the  
 111 activation process (e.g., heat transfer process if thermal activation was used) and assumes that the  
 112 deformed shape could be perfectly “locked in” once activation is removed. However, these behaviors  
 113 could be included in the forward modeling in subsequent work without significant change to the  
 114 computational design strategy. Similarly, the overall dimensions of the tile were assumed to be  
 115 given/fixed. Thus, the remaining unknown variables to determine for the design of this tile concept  
 116 are the locations and magnitude of mechanical actuation (i.e., applied force and/or displacement)  
 117 and the location and size of the regions of the material to be activated.

## 118 DESIGN SOLUTION STRATEGY

119 The design strategy considered herein is based on utilizing non-linear optimization in combi-  
 120 nation with a numerical representation of the shape changing tile to be designed. As noted, the  
 121 primary objective of the optimal design is to achieve a given desired shape change. In this work, the  
 122 target shape was assumed to be defined as the desired outer surface shape of the tile. However, as is  
 123 often the case with smart material applications, minimizing the energy cost of the shape changing  
 124 process was also considered as an objective of the design. Thus, the design problem can be written  
 125 in the general form of the following constrained optimization problem:

$$\begin{aligned}
 & \underset{\vec{\gamma}}{\text{minimize:}} && \{C(S_T, S_F(\vec{u})), E(\vec{u}, \vec{\gamma})\} \\
 & \text{subject to:} && F(\vec{u}, \vec{\gamma}) = 0 \\
 & && \vec{b}_l \leq A(\vec{\gamma}) \leq \vec{b}_u,
 \end{aligned} \tag{1}$$

127 where  $S_T$  is the target surface shape,  $S_F$  is the predicted morphed shape of tile as defined by

128 the deformation of the tile,  $\vec{u}$ , estimated by the solution of the forward problem,  $F(\vec{u}, \vec{\gamma}) = 0$   
129 (i.e., the partial differential equation constraint), for a given set of actuation and activation design  
130 parameters,  $\vec{\gamma}$ ,  $C(\cdot, \cdot)$  is the metric that quantifies the difference between two shapes,  $E(\vec{u}, \vec{\gamma})$  is the  
131 estimated energy consumption required to complete the shape change process,  $\vec{b}_l$  and  $\vec{b}_u$  are the  
132 lower and upper bound constraint vectors, respectively, and  $A(\vec{\gamma})$  is the operator that forms the  
133 necessary constraint equations involving the design parameters. Note that this is the general form  
134 of the optimization problem considered herein, and the examples will more specifically state the  
135 respective components, including the example-specific objective functions, design parameters, and  
136 constraints utilized.

137 An estimate of the optimal design solution can be found through any preferred optimization  
138 strategy applied to Equation 1 to determine the actuation and activation parameters (within the  
139 physical bounds) that minimizes the difference between the deformed tile shape predicted by  
140 the forward problem and the target shape. Both standard gradient-based and non-gradient-based  
141 optimization strategies were utilized in the present study, with specific details provided in the  
142 Examples Section. As noted, specific focuses of the development were the shape difference metric  
143 and the parameterization strategy, which are discussed in more detail in the following.

### 144 **Shape Difference Metric**

145 There are multiple methods of shape description that can be used to quantify the difference  
146 between two shapes. In general, shape descriptors are separated into two categories: region-  
147 based shape descriptors (Lu and Sajjanhar 1999; Zhang and Lu 2004; Veltkamp 2001), which  
148 calculate the descriptor based on the entire volume of a shape, and contour-based shape descriptors  
149 (Veltkamp 2001), which calculate the descriptor based solely on the contour (or boundary) of the  
150 shape. Generally, region-based shape descriptors are not well suited for this type of application and  
151 so only contour-based descriptors were considered. Specifically, a sub-category of contour-based  
152 shape descriptors, correspondence-based shape descriptors, were considered.

153 One relatively intuitive correspondence-based approach is to project the target shape onto the  
154 initial tile shape (i.e., flat tile) to establish a point-to-point correspondence, and then measure the

155 difference between the location of the surface points on the target shape and the deformed location  
 156 of the surface points estimated for a given design solution for all of these now corresponding points.  
 157 Specifically for this work, a projection-based metric for a discretized tile surface was defined as:

$$158 \quad PM_d = \sum_{i=1}^{N_C} \| \vec{x}_{Si} - \vec{x}_{Fi} \|, \quad (2)$$

159 where  $\vec{x}_{Si}$  and  $\vec{x}_{Fi}$  are the spatial coordinates on the target shape and deformed tile shape from the  
 160 design estimate, respectively, for the  $i^{th}$  point in the correspondence set,  $N_C$  is the number of points  
 161 in the point-to-point correspondence, and  $\| \cdot \|$  is the Euclidean distance. Other similar approaches  
 162 that first form a set of corresponding points between a target shape and an estimated morphed  
 163 structure shape have been used in similar design applications (Lu and Kota 2003). However, these  
 164 approaches can potentially limit the design space as they conceptually change the design problem to  
 165 matching a desired displacement of certain points rather than a more general shape. Furthermore,  
 166 the projection strategy considered here to form the correspondence is only applicable to target  
 167 shapes with non-overlapping regions so that a one-to-one correspondence is formed. Alternatively,  
 168 the Hausdorff distance and similar variants have been developed to quantify the difference between  
 169 two shapes in a more general sense and with no limitation on the type of shapes being compared  
 170 (Veltkamp 2001; Huttenlocher et al. 1993).

171 Assuming the shapes are discretized, the Hausdorff distance is a point-to-point matching that  
 172 finds the maximum closest pairing between all the points on each shape. The Hausdorff distance  
 173 between two shapes discretized into two collections of points  $S_1$  and  $S_2$  is defined as:

$$174 \quad H_d(S_1, S_2) = \max(D(S_1, S_2), D(S_2, S_1)), \quad (3)$$

$$175 \quad \text{where: } D(S_1, S_2) = \max_{\vec{x}_1 \in S_1} \min_{\vec{x}_2 \in S_2} \| \vec{x}_1 - \vec{x}_2 \|, \quad (4)$$

177  $\vec{x}_1$  is the collection of points in shape  $S_1$ ,  $\vec{x}_2$  is the collection of point in shape  $S_2$ , and again  $\| \cdot \|$   
 178 is the Euclidean distance. A visual representation of  $D(S_1, S_2)$  and  $D(S_2, S_1)$  can be seen in Figure

179 2. An important note is that this Standard Hausdorff distance defined by Equation 3 can suffer  
 180 from over-sensitivity to outliers, which can be expected as the Hausdorff distance is analogous to  
 181 a  $L_\infty$  norm. To address these issues with the Hausdorff distance several modified versions have  
 182 been developed and explored (Dubuisson and Jain 1994). For the present study the best performing  
 183 modification in (Dubuisson and Jain 1994) was also considered alongside the Standard Hausdorff  
 184 distance and the projection-based distance which can be defined as:

$$185 \quad MH_d(S_1, S_2) = \max(M(S_1, S_2), M(S_2, S_1)) \quad (5)$$

$$186 \quad \text{where: } M(S_1, S_2) = \frac{1}{N_1} \sum_{i=1}^{N_1} \min_{\vec{x}_2 \in S_2} \|\vec{x}_1 i - \vec{x}_2\|, \quad (6)$$

188  $N_1$  is the number of points on shape  $S_1$ ,  $\vec{x}_1 i$  is the  $i^{th}$  point in  $\vec{x}_1$ , and  $N_2$  is the number of points  
 189 on shape  $S_2$ . This Modified Hausdorff distance is analogous to an  $L_1$  norm and ensures that every  
 190 point on each shape contributes to the distance metric.

## 191 **Actuation and Activation Parameterization**

192 When considering the computational design of a smart material structure such as the proposed  
 193 SMP building tile, there are many methods available to activate and actuate the structure to achieve  
 194 the desired behavior. Generally, in similar applications the entirety of the smart material is activated.  
 195 However, additional functionality can be achieved through a mixture of smart material and a passive  
 196 material, such as in (Peraza-Hernandez et al. 2013) which considered a Shape Memory Alloy (SMA)  
 197 mesh binded to a passive material to achieve a self-folding structure. Alternatively, others have  
 198 considered partial (or localized) smart material activation to increase functionality (Wang and  
 199 Brigham 2012). As the activation process was not included in the system model for the work  
 200 herein, there is no difference conceptually in the optimal design procedure whether the intention is  
 201 to use localized activation or to combine active and passive materials. In both cases, the objective  
 202 of the activation portion of the optimal design are the same, which is to define the distribution (i.e.,  
 203 size and location) of the regions of the structure that would have the activated (i.e., soft) material  
 204 properties.



205 For any inverse problem where the objective is to obtain the material property distribution, there  
206 are many different ways to parameterize the unknowns. The main concern with the parameterization  
207 is often the trade-off between generality (i.e., being able to capture any possible distribution) and  
208 computational expense. The more general the parameterization the higher the computational  
209 expense of the problem. For example, finite element-type discretizations of a material property  
210 distribution (Wang et al. 2015), for which every node or element of a mesh can have a different  
211 property, have a high degree of general applicability. However, the large number of unknowns in  
212 a mesh description can substantially increase computational expense and may require some kind  
213 of regularization or other additional consideration to address ill-posedness. Alternatively, many  
214 lower-dimensional parameterizations have been considered to reduce computational expense and  
215 avoid ill-posedness, such as the use of radial basis functions (Ahmadpoor et al. 2016). The challenge  
216 with lowering the dimension of the parameterization is that it is often problem-dependent and best  
217 used when some *a priori* information is available or can be estimated regarding the expected type  
218 of spatial distribution.

219 In order to balance computational cost with generality for this specific application, the distribu-  
220 tion of activated material was parameterized into a fixed number of activated regions, assuming the  
221 material would be activated uniformly through the thickness. The number of regions was chosen  
222 to be sufficiently large to allow for complex solutions (e.g., many disconnected activated regions),  
223 but the regions could overlap to allow for simple solutions as well (e.g., a single local activated  
224 region). Furthermore, a threshold was set so that any small gaps between activated or inactivated  
225 material regions would be removed to improve practicality of the design solutions. Thus, the ma-  
226 terial distribution was defined by  $m$  discrete activated material sections centered at variable planar  
227 locations,  $\{d_j\}_{j=1}^m$ , along the tile with variable widths/diameters,  $\{l_j\}_{j=1}^m$ . An important note is that  
228 this parameterization of the material activation is expected to lead to non-unique solutions in terms  
229 of the parameters, even for cases where there is one optimal distribution of material properties.  
230 However, this non-uniqueness was not a concern, since the distribution and not the parameters  
231 themselves is the important outcome, and uniqueness in optimal design problems is generally not

critical. The actuation was chosen to be implemented through variable applied pressure and a series of  $n$  discrete actuators at variable planar locations,  $\{c_i\}_{i=1}^n$ , and with variable horizontal and vertical prescribed displacements,  $\{u_i\}_{i=1}^n$  and  $\{w_i\}_{i=1}^n$ , respectively. Figure 3 shows a two-dimensional (2D) schematic of the tile with an applied pressure  $P$ ,  $n$  discrete actuators, and  $m$  discrete activated zones for a maximum of  $3n + 2m + 1$  potential design variables to be determined.

## RESULTS AND DISCUSSION

Several numerical case studies of the design of a smart material shape changing tile were considered to evaluate the capability of the shape-based optimal design strategy presented to achieve nontrivial design solutions and examine any potential benefits or limitations for the various component options discussed. In all examples the conceptual shape-changing tile was taken to be 10.16 *cm*-by-10.16 *cm* (4 *in*-by-4 *in*) with a thickness of 0.25 *cm* (0.1 *in*) and the activated and inactivated mechanical material properties were based upon those for a standard shape memory polymer (SMP) (Beblo et al. 2010). Although it is not expected that such a material would be suitable for architectural applications without further development/modification, the shape memory and large recoverable strain capabilities of SMP (Leng et al. 2011) would be significantly beneficial for the proposed concept of a shape changing building skin tile. Therefore, SMP was chosen as the exemplar smart material for the development of this concept. The material was assumed to be an isotropic Neo-Hookean hyperelastic material model with activated and inactivated Young's moduli of 2.4 *MPa* and 1034 *MPa*, respectively, and a constant Poisson's ratio of 0.45. The process to change the shape (i.e., deform) the tile was assumed to be quasi-static. As previously noted, the material was assumed to be activated instantaneously so that regions of the tile were either activated or inactivated completely, and it was further assumed that all activation of material occurred prior to the application of any actuation. A final important consideration not yet mentioned for the design of this type of smart material shape-changing structure is to ensure that the design solution does not damage the structure. Although a constraint could be included in the design optimization problem to prevent solutions that damage the material (Wang and Brigham 2012), preliminary tests showed this to be unnecessary for the case studies considered. However, the final design solutions were still

259 checked to ensure no damage of the material would occur by confirming the maximum principal  
260 strain did not exceed damage limits anywhere of 30% for inactivated material or 400% for activated  
261 material.

262 In addition to the capability to identify nontrivial design solutions to complex problems, a  
263 primary benefit of a computational design approach such as that proposed is the generalisability in  
264 contrast to more traditional design strategies. Therefore, the focus of the test cases used to evaluate  
265 the capability of this approach was not just to show that the approach could be successfully applied  
266 to the morphing façade tile concept, but to also show the range of applicability without the need  
267 to fundamentally change the solution strategy. In particular, the examples chosen focused on the  
268 capability to identify relatively high-quality design solution regardless of the fundamental nature  
269 of the topology (assuming a continuous surface) and the degree of spatial variability of the desired  
270 surface shape, while also including a range of actuation and activation types and constraints, and  
271 being able to incorporate additional design objectives (not just a target shape).

272 To explore variations in the fundamental topology of the target shape for the morphing structure,  
273 two classes of target shapes were considered: (1) convex surfaces (for which the projection strategy  
274 for the design objective would be applicable) and (2) non-convex surfaces. In addition, within each  
275 of these classes one target shape was considered with a “smooth” spatial variation and another  
276 non-smooth target shape with “sharp” changes in the surface was considered to see if this aspect  
277 also had an effect on the solution capability. The majority of the test cases considered one direction  
278 of spatial variability for the target shape (i.e., two-dimensional target shapes). However, to also  
279 show that the design approach generalizes to a higher degree of spatial variability, one additional  
280 test case was considered for a target shape with two directions of spatial variability (i.e., a three  
281 dimensional target shape).

282 Throughout the test cases, the independence of the solution strategy with respect to the design  
283 parameters (i.e., activation and actuation) is shown by changing both the number of discrete  
284 design parameters and the physical property these parameters define. Initially, the actuation of the  
285 morphing structure is fixed and the design parameters only relate to the number and location of

286 actuators. Then, the capability of the morphing structure to have variable actuation was included,  
287 and these new design parameters defined the location and size of the activated material. The case  
288 of variable actuation also facilitated the consideration of additional design problem objectives (in  
289 addition to the target shape), as energy cost would be a potentially important design component for  
290 a morphing structure and amount of material activated can often represent the largest energy cost.  
291 Thus, the design approach was modified to account for multiple objectives, the target shape and  
292 the energy cost, and the capability of the computational approach to elucidate the range of design  
293 solutions with respect to multiple objectives and their corresponding trade-off is shown.

294 Table 1 shows the design cases considered in the order they appear and their corresponding  
295 topology classification, the design parameters to be determined, and the design objectives consid-  
296 ered (as well as whether single or multi-objective design). More details of the case studies will be  
297 given in their respective sections.

### 298 **Capability of a Shape-Based Objectives for Optimal Design**

299 In Cases 1 and 2 the capability of the correspondence-based shape difference metrics as objective  
300 functions to accurately match a target shape were investigated. For both of these cases, the tile  
301 was assumed to be fully activated (i.e., the only optimization parameters to be considered were  
302 the mechanical actuation variables) to simplify the design solution space, so that the capability of  
303 the various objective functions could be more easily compared. Full activation was considered to  
304 focus on the design objective functions, rather than comparing the capabilities of local to global  
305 activation. Furthermore, energy cost was ignored for these first tests (i.e., not included in the  
306 optimization), since the activation energy is typically the primary energy cost and was not varying  
307 for these tests.

308 For both Cases 1 and 2, a constrained gradient-based interior point algorithm was used to solve  
309 Equation 1 by minimizing  $C(S_T, S_F(\vec{u}))$  (removing the energy term from Equation 1). For each  
310 numerical example, the gradient-based optimization was repeated with 10 randomly generated  
311 initial guesses and the solution was taken to be the result with the lowest respective objective  
312 function value. The optimization stopping criteria was set to be when the change in objective

313 function between iterations fell below the tolerance value of  $10^{-6}$ . Starting with one actuator, the  
314 number of actuators for the design was increased by one and the optimization repeated until the  
315 shape matching capability did not noticeably improve (i.e., convergence was achieved in terms of  
316 the number of actuators). This type of optimization was done for simplicity since the parameter  
317 for the number of actuators is an integer, while the remaining design parameters are continuous  
318 real numbers. Each of the correspondence-based objective functions defined in Section 3, the  
319 Standard Hausdorff distance, the Modified Hausdorff distance, and the projection-based distance,  
320 were used in turn as the objective function for the optimization process. In order to have a fair  
321 comparison between each of the potential design solutions, regardless of the objective function  
322 used in the optimization process, the Standard Hausdorff distance and Modified Hausdorff distance  
323 were calculated for the final designed tile shapes in comparison to the target shapes. The design  
324 problem was constrained to be two-dimensional by assuming both the activation and actuation  
325 would be constant in one planar direction. Additionally, for Cases 1 and 2 the two end faces of the  
326 tile that were parallel to the direction of constant activation and actuation were taken to be fixed  
327 with zero displacement in all directions (as shown in Figure 3), while all other faces were free to  
328 deform due to the actuation detailed in Section 3.

### 329 *Convex Target Shapes*

330 Figure 4 shows the two target shapes considered in this case, an “overhang” shape (Target  
331 Shape 1) and a unidirectional sin-wave (Target Shape 2) for this case. Both shapes were based  
332 upon work in (Zupan et al. 2018), which detailed the self-shading performance of these shapes in a  
333 similar application for a building skin. Both target shapes are convex with one direction of spatial  
334 variability. Target Shape 1 had a flat (i.e., undeformed) cross-section for half of the tile, and the  
335 other half had a cross-section defined by a single sin wave with amplitude  $4.57\text{ cm}$  and a period  
336 of  $5.08\text{ cm}$ , due to the discontinuity this shape is considered “non-smooth”. Target Shape 2 was  
337 defined by a sin wave cross-section with amplitude  $2.74\text{ cm}$  and a period of  $5.08\text{ cm}$ , this shape is  
338 considered “smooth”.

339 Figure 5 shows the Standard and Modified Hausdorff distances for the final design shapes

340 obtained from optimizing with respect to each of the correspondence-based objective functions  
341 with one through five discrete actuators for Target Shapes 1. No sufficiently accurate solution could  
342 be found for a one actuator design, which is consistent with intuition. However, all design solutions  
343 that utilized two or more actuators for Target Shape 1 resulted in Standard and Modified Hausdorff  
344 distances less than 10% the length increase (2.08 *cm*) of the tile, with only the exception of the four  
345 actuator case using the Standard Hausdorff objective function that had a slightly higher error. In  
346 other words, the design solution converged at two actuators for Target Shape 1. The shape matching  
347 for Target Shape 1 when minimizing with respect to all three objective functions can be seen in  
348 Figure 6, which shows the final deformed shape and the design solution (i.e., actuator placement  
349 and pressure) corresponding to each objective function. Clearly, designs that can accurately match  
350 the target shape were able to be obtained when they existed, regardless of the specific shape-based  
351 objective function utilized in this case. The convergence at two actuators is expected based on  
352 the key features of the shape (i.e., one actuator to hold the first half of the tile in place and a  
353 second actuator to define the height of the “overhang”). Also of note, there are fluctuations in  
354 the Standard and Modified Hausdorff distances for the final design shapes, most notably for the  
355 solutions obtained by minimizing the Standard Hausdorff distance. The larger fluctuations in the  
356 solutions, imply that the Standard Hausdorff Distance creates a more complex solution space that is  
357 more difficult for an optimization algorithm to traverse (i.e., more local minima exist in comparison  
358 to the other objective functions).

359 The results for Target Shape 2 were similar to those for Target Shape 1, but accurate design  
360 solutions were not able to be obtained until at least 3 actuators were utilized (Figure 7). The shape  
361 matching for Target Shape 2 when minimizing with respect to all three objective functions can be  
362 seen in Figure 8, which shows the final deformed shape and the design solution corresponding to  
363 each objective function. A main difference in the results for Target Shape 2 is that an odd number  
364 of actuators were necessary to accurately match the desired shape, with even numbers of actuators  
365 resulting in errors as high as 300% more than when using an odd number of actuators. This is due  
366 to the need for an odd number of actuators to be able to match the key features of a symmetric

367 shape, by placing one actuator at the line of symmetry and an equal number on each side of the  
368 line of symmetry. Consistent with the results from Target Shape 1, the Standard Hausdorff distance  
369 objective function resulted in a more challenging optimization problem and led to the identification  
370 of inaccurate design solutions in terms of the shape matching for some cases of Target Shape 2.

371 An important note is there are design solutions that have nearly identical actuator placements  
372 and deformations, but substantially different applied pressure values for both Target Shapes 1 and  
373 2, as seen in Figures 6 and 8. This could be interpreted as the pressure variable being a superfluous  
374 variable in the design of the shape changing mechanisms and should likely be removed from the  
375 system if implemented for these cases. However, as will be shown in the following, the ability  
376 to control an applied pressure became significant for more complicated target shapes and when  
377 utilizing localized activation.

### 378 *Non-Convex Target Shapes*

379 Figure 9 shows the two target shapes considered in this case, a boxcar function (Target Shape  
380 3) and a distorted sin-wave (Target Shape 4), for this case. Both target shapes are non-convex  
381 with one direction of spatial variability. Target Shape 3 was a centered boxcar function with a  
382 width of 5.08 *cm* and a height of 2.54 *cm*, due to the discontinuities in the shape it is considered  
383 “non-smooth”. Target Shape 4 was a centered sin-wave with an amplitude of 2.62 *cm* and a  
384 period of 10.16 *cm*, which was rotated 75° about the out-of-plane axis, this shape is considered  
385 “smooth”. As projection is not applicable for these shapes, only the Standard and Modified  
386 Hausdorff distances were used as objective functions within the design optimization procedure for  
387 this case. Additionally, in these examples the number of actuators was incremented from one to  
388 seven, due to the increased target shape complexity.

389 Figures 10 and 11 show the Standard and Modified Hausdorff distances for the final design  
390 shapes obtained from optimizing with respect to those same two applicable correspondence-based  
391 objective functions with one through seven discrete actuators for Target Shapes 3 and 4, respectively.  
392 Even with the substantial increase in target shape complexity, solutions that clearly matched Target  
393 Shapes 3 and 4 could be found. The sufficiency of the design solutions can be visually confirmed

394 through Figures 12 and 13, which show the final deformed shapes and design solutions correspond-  
395 ing to each objective function. Even though the optimization process typically converged to a design  
396 solution with a higher error than the prior set of examples (e.g., error values of approximately 10%  
397 of the length change of the tile), the optimization process using the Modified Hausdorff distance  
398 led to design solutions that matched both of the complex target shapes accurately. Alternatively,  
399 the limitation of the Standard Hausdorff distance that resulted in less consistent optimization was  
400 even more significant, with the corresponding design solutions for Target Shapes 3 and 4 being  
401 substantially less accurate, both quantitatively and visually.

402 Regarding the design variables, as expected the optimal design process revealed that this more  
403 complex second set of target shapes required more actuators (four or five) in comparison to the  
404 prior example set (two or three actuators) to accurately match the desired shapes. Additionally, in  
405 contrast to the previous set of examples, the pressure design variable was an important variable to  
406 the design, and consistent pressure values were identified for the design solutions that accurately  
407 matched the target shapes.

### 408 **Locally Activated Shape Changing Tile**

409 After establishing the capabilities of the shape difference metrics, Case 3 focused on the use  
410 of localized material activation for the design of a smart material shape-changing structure. To  
411 investigate the optimal design problem now with localized material activation rather than full  
412 activation, a subset of the target shapes from both of the prior test sets were considered: Target  
413 Shape 2 (unidirectional sin-wave, Figure 4(b)) and Target Shape 4 (distorted sin-wave, Figure 9(b)).

414 To contrast with the previous results with full activation in terms of shape matching accuracy,  
415 an optimization process similar to the previous two cases (a constrained gradient-based interior  
416 point algorithm) was utilized to find design solutions. The localized activation was implemented  
417 as described in Section 3. Due to prior results showing higher accuracy, the Modified Hausdorff  
418 distance was the only shape metric considered in this case.

419 Figures 14(a) and 14(b) show the value of the Modified Hausdorff distance for the final design  
420 shapes obtained from optimizing with respect to the Modified Hausdorff distance with one through



421 four discrete actuators for Target Shapes 2 and 4 for both localized activation and full activation  
422 (i.e., the same as those shown in Figures 7 and 11). Specifically, in Figure 14(a) it can be seen that,  
423 with the exception of one actuator, the optimization procedure that included localized activation  
424 found design solutions that resulted in lower Modified Hausdorff distance values (i.e., better shape  
425 matching) for Target Shape 2 than when using full activation. Similarly considering Target Shape 4  
426 (Figure 14(b)), the optimal designs utilizing localized material activation resulted in lower Modified  
427 Hausdorff distance values for every design case. The design solutions using localized activation  
428 were even capable of improving the shape matching for Target Shape 4 using less actuators (e.g.,  
429 one actuator with localized activation was more accurate than four actuators with full activation).  
430 This shows that the design strategy was able to determine these non-intuitive (based on previous  
431 results) solutions when including localized activation. Thus, there is clear benefit to the use of  
432 localized activation to achieve improved shape matching of a smart material morphing structure.  
433 Moreover, the use of less actuators to achieve a more accurate shape indicates that the use of  
434 localized activation is not only beneficial for shape matching purposes but also does so with a lower  
435 energy cost in terms of both thermal activation and mechanical actuation.

### 436 **Target Shape with Two Directions of Spatial Variability**

437 For this group of numerical case studies, the same approach for the design optimization as the  
438 first group of tests was used (interior point algorithm minimizing shape difference) with the Modified  
439 Hausdorff distance used as the objective function. The same concept of variable parameterization  
440 was used as for the previous examples, however the discrete actuators were removed from the design  
441 space in order to reduce the complexity of the design space (i.e., the only actuation was the applied  
442 pressure). The activation was defined by a set of circular regions on the 3D tile, activating uniformly  
443 through the thickness as before, with controllable center locations and diameters. Differing from  
444 the previous three groups of tests (which had 2 fixed edge faces and 2 free edge faces), all four outer  
445 edge faces were fixed to have zero displacement in all directions and the target shape considered  
446 has two directions of spatial variability.

447 Figure 15 shows the target shape, a boxcar function extended to three dimensions. The boxcar

448 portion of the target shape had a height of  $1.27\text{ cm}$  and was centered on the lines  $x = 1.27\text{ cm}$  and  
449  $y = 0\text{ cm}$  with a width of  $2.54\text{ cm}$  and a length of  $7.62\text{ cm}$ . This target shape was chosen to be  
450 similar to an overhang shape (a common shading device).

451 Figure 15 shows the location of the activated material for the final design solution. These  
452 activated regions are concentrated over the location of the boxcar portion of the target shape,  
453 which is consistent with what would be expected given the constraints on the design problem. The  
454 Modified Hausdorff distance between the deformed model surface and the 3D target shape for this  
455 design solution was  $0.20\text{ cm}$ . A plot of a cross-section (taken at  $y = 0\text{ cm}$ ) of the target shape and  
456 the deformed model surface of the design solution is shown in Figure 17. In this case the design  
457 optimization was not able to reach a solution with the sharp features of the 3D target shape. This  
458 is due to only using a uniform pressure which will always result in a smooth, continuous solution.  
459 However, the Modified Hausdorff distance of  $0.20\text{ cm}$  can be considered a small value, particularly  
460 in comparison to the prior examples in Section 4, which has Modified Hausdorff distance values of  
461  $0.20\text{ cm}$  for two or more actuators. Furthermore, although the deformed tile is observably different  
462 than the 3D target shape, this design solution still resembles an overhang, which was the goal of  
463 choosing the target shape in the first place.

#### 464 **Multi-Objective Design - Shape Difference and Energy Cost**

465 When utilizing local activation, the energy cost to change the structure's shape varies far more  
466 significantly depending upon the design than for the previous cases. Therefore, to explore the  
467 capability to design utilizing additional objectives (in addition to the shape targeting) energy was  
468 included as an objective in Case 5.

469 For this multi-objective case a controlled, elitist genetic algorithm (Guide 1998) was used  
470 to solve Equation 1 by simultaneously minimizing both  $C(S_T, S_F(\vec{u}))$  and  $E(\vec{u}, \vec{\gamma})$  to determine  
471 potential design solutions. The initial population was set to be 200 and the stopping criteria was  
472 set as either a maximum number of generations of  $200 * N_D$  (where  $N_D$  is the number of design  
473 variables) or when the objective function difference between iterations fell below a tolerance of  
474  $10^{-4}$ ). The result of the multi-objective optimization for each trial was the Pareto front set of

475 solutions. The Pareto front includes all of the “best” potential design solutions within the limit of  
 476 the population size that have a lower value for at least one of the separate objective functions in  
 477 comparison to any other solution estimate seen throughout the optimization process. This Pareto  
 478 front is particularly useful to analyze the trade-off between the two objectives, shape matching  
 479 accuracy and energy cost. Similar to the first three cases of numerical tests the design problem was  
 480 again constrained to be two dimensional and have the same boundary conditions.

481 As the Modified Hausdorff distance was universally applicable and led to substantially more  
 482 consistent design solutions compared to the other objectives considered, this was the only shape-  
 483 based objective function used for the following case. Based on the example of a thermally activated  
 484 SMP, the energy required to morph the smart material tile in this application could be quantified  
 485 from the design pressure, mechanical actuation, and material activation as follows:

$$486 \quad E = \int_{\Gamma} P(-\vec{n} \cdot \vec{u})d\Gamma + \sum_{i=1}^n \vec{F}_i \vec{u}_i + c_p \rho V_a \Delta T, \quad (7)$$

487  $\vec{n}$  is the unit outward normal to the tile surface where pressure was applied,  $\Gamma$ ,  $\vec{u}$  is the displacement  
 488 vector,  $\vec{F}_i$  is the resultant force vector needed to displace the  $i^{th}$  mechanical actuator by  $\vec{u}_i$ ,  $c_p$  is  
 489 the specific heat of the SMP (taken as  $c_p = 2009 \frac{J}{kg-K}$ ),  $\rho$  is the density of the SMP (taken as  
 490  $\rho = 35.98 \frac{kg}{m^3}$ ),  $\Delta T$  is the temperature change required to activate the material, and  $V_a$  is the volume  
 491 of the tile that is activated (determined based on the activated zone parameterization defined in  
 492 Section 3). As noted previously, the activation process was not considered within this study.  
 493 Therefore, to quantify the energy to activate the material, it was assumed that the activated zones  
 494 would have to be heated from room temperature ( $18^\circ C$ ) to the SMP activation temperature of  $25^\circ C$ ,  
 495 resulting in a fixed temperature change for the activated zones of  $\Delta T = 7^\circ C$ .

496 The target shapes considered for Case 5 were again a subset of the previous shapes considered,  
 497 specifically Target Shapes 2 (Figure 4b) and 4 (Figure 9b). The design strategy was capable of  
 498 finding Pareto fronts for both of the target shapes considered in Case 5. Figure 18 shows the  
 499 composite Pareto fronts in terms of the total energy cost and final Modified Hausdorff distance

500 for the potential designs obtained from the multi-objective optimization for Target Shapes 2 and  
501 4. These composite Pareto fronts were constructed from the final populations of potential design  
502 solutions for each case of one through five actuators. One method for choosing the preferred  
503 solution (i.e., single optimal solution) from a Pareto front is to select the solution that is nearest to  
504 the origin along the front. The two optimal design solutions (one for each Target Shape) that were  
505 nearest to the Pareto front origin are shown in terms of the deformed shapes, actuator placements,  
506 and activated zones in Figures 19 and 20.

507 Both Pareto fronts determined from the design strategy corresponding to Target Shape 2 and  
508 4 show a distinct point of diminishing returns in terms of both objectives, with each Pareto front  
509 having a clear L-shape. For example, for Target 2 in order to reduce the energy cost by 30%  
510 from the optimal solution on the L-shaped curve the accuracy of the shape matching must be  
511 reduced by 173%. Similarly, in order to improve the shape matching accuracy by 4% from the  
512 optimal solution, the energy cost increases by 17%. To examine the design solutions further,  
513 the relative contribution of the mechanical actuation and the material activation to the morphing  
514 energy cost was examined for each case. It was found that the material activation energy cost was  
515 significantly greater than the mechanical actuation energy cost in all cases, but the extent of which  
516 was dependent on the number of actuators utilized for the design. Specifically, when one actuator  
517 was utilized the thermal energy cost was greater than 90% of the total energy cost while it was as  
518 low as 60% of the total energy cost while utilizing five actuators. Thus, there were at times highly  
519 non-intuitive outcomes in balancing the number of actuators, total energy cost, and shape accuracy  
520 that the design strategy was able to determine. Further related to energy efficiency, Figures 19  
521 and 20 show that even though 20 separate activated zones ( $m = 20$ ) could be utilized, the push for  
522 efficiency naturally led to smooth (i.e., a small number of continuous activated regions rather than  
523 a large number of small activated zones) results, and in affect, regularized the solution (eliminating  
524 the need for regularization of the parameterization). Looking more closely at the Pareto front  
525 corresponding to Target Shape 2 (Figure 18(a)), the solutions clustered around the point nearest  
526 the Pareto front origin generally utilized three or five actuators, while the solutions with higher

527 Modified Hausdorff distance values and lower energy cost utilized a mixture of one, two, and four  
528 actuators. Considering the Pareto front corresponding to Target Shape 4 (Figure 18(b)), it was  
529 found that all solutions with a Modified Hausdorff distance below 0.19 *cm* utilized four actuators,  
530 while the remainder utilized two actuators. Again, the fluctuations in the solutions are non-intuitive  
531 in comparison to the previous single objective optimization and indicate the necessity of a design  
532 approach, such as that presented, for maximum shape matching and energy cost benefits.

## 533 **CONCLUSIONS**

534 The development and evaluation of a computational approach for optimal design of a smart  
535 material shape changing building skin tile was presented. This approach was evaluated through  
536 numerical examples that considered the capability of the computational procedure while utilizing  
537 various shape-based objectives and design variable parameterizations to accurately match target  
538 shapes with a variety of features (convex/non-convex, smooth/non-smooth, and one/two directions  
539 of spatial variability). The results from the design approach indicated that the computational  
540 approach utilizing the shape-based objective functions can result in mechanisms of morphing that  
541 lead to accurate deformed shapes in comparison to various target shapes. Of the shape metrics  
542 considered, the Modified Hausdorff distance was shown to be preferable because the computational  
543 approach utilizing the Modified Hausdorff distance resulted in the most consistently accurate shape  
544 matching. Additionally, the computational approach utilizing the Modified Hausdorff distance was  
545 applicable to any shape, even non-convex target shapes, while retaining acceptable deformed shape  
546 accuracy. The results from the design approach also indicated that the use of localized material  
547 activation for the design of a smart material shape changing structure of the type considered here  
548 can lead to higher accuracy in matching target shapes (i.e., better functionality) than a design  
549 that only has the capability to activate the entire structure. However, the design space for the  
550 system considered had a significant trade-off between shape matching accuracy and energy cost.  
551 Yet, the ability to use localized activation for the design was shown to require considerably less  
552 energy to perform the shape change and to require less actuation devices, potentially benefiting  
553 implementation considerably.

554 One limitation of this approach is the computational expense of using the Hausdorff distance  
555 or its variants for the optimization objective function. This computational expense could become  
556 particularly prohibitive if considering a more complex structure that required a more time consum-  
557 ing forward analysis and/or if the number of design parameters increased significantly. However,  
558 there are several possibilities to improve the computational efficiency of the solution strategy. One  
559 approach is to develop and use differentiable forms of the Hausdorff metrics so that direct differ-  
560 entiation, or even an adjoint approach could be used for gradient calculation during optimization  
561 rather than finite difference. Additionally, reduced-order or surrogate modelling approaches could  
562 be used to complement or replace the standard finite element analysis utilized in this study to  
563 substantially reduce the computational expense of forward analysis.

#### 564 **ACKNOWLEDGMENTS**

565 The authors gratefully acknowledge the financial support of the National Science Foundation  
566 through Award No. 1536797.

## REFERENCES

- Ahmadpoor, M., Notghi, B., and Brigham, J. C. (2016). "A generalized iterative approach to improve reduced-order model accuracy for inverse problem applications." *Journal of Engineering Mechanics*, 142(5), 04016020.
- Barrett, R. M. and Barrett, R. P. (2016). "Thermally adaptive building covering field test." *Procedia Engineering*, 145, 26–33.
- Beblo, R., Gross, K., and Mauck Weiland, L. (2010). "Mechanical and curing properties of a styrene-based shape memory polymer." *Journal of Intelligent Material Systems and Structures*, 21(7), 677–683.
- Bridgens, B. (2018). "Hygromorphic tile concept, <<https://blogs.ncl.ac.uk/responsive-materials>>.
- Cilento, K. (2012). "Al bahar towers responsive facade/aedas." *ArchDaily*, 'September, 5.
- Clifford, D. (2019). "Cactus tile concept, <<http://cmubiologic.weebly.com/cactus-tile.html>>.
- Dewidar, Y., Mohamed, N., and Ashour, Y. (2013). "Living skins: A new concept of self active building envelope regulating systems." *Advancing the Green Agenda; Technology, Practices and Policies Conference–BUID*, 1–8.
- Dubuisson, M.-P. and Jain, A. K. (1994). "A modified hausdorff distance for object matching." *Pattern Recognition, 1994. Vol. 1-Conference A: Computer Vision & Image Processing., Proceedings of the 12th IAPR International Conference on*, Vol. 1, IEEE, 566–568.
- Guide, M. U. (1998). "The mathworks." *Inc., Natick, MA*, 5, 333.
- Holstov, A., Bridgens, B., and Farmer, G. (2015). "Hygromorphic materials for sustainable responsive architecture." *Construction and Building Materials*, 98, 570–582.
- Huttenlocher, D. P., Klanderman, G. A., and Rucklidge, W. J. (1993). "Comparing images using the hausdorff distance." *IEEE Transactions on pattern analysis and machine intelligence*, 15(9), 850–863.
- Jani, J. M., Leary, M., Subic, A., and Gibson, M. A. (2014). "A review of shape memory alloy research, applications and opportunities." *Materials & Design (1980-2015)*, 56, 1078–1113.
- Lampert, C. M. (2004). "Chromogenic smart materials." *Materials today*, 7(3), 28–35.

594 Leng, J., Lan, X., Liu, Y., and Du, S. (2011). "Shape-memory polymers and their composites:  
595 stimulus methods and applications." *Progress in Materials Science*, 56(7), 1077–1135.

596 Liu, Y., Du, H., Liu, L., and Leng, J. (2014). "Shape memory polymers and their composites in  
597 aerospace applications: a review." *Smart Materials and Structures*, 23(2), 023001.

598 Lu, G. and Sajjanhar, A. (1999). "Region-based shape representation and similarity measure suitable  
599 for content-based image retrieval." *Multimedia Systems*, 7(2), 165–174.

600 Lu, K.-J. and Kota, S. (2003). "Design of compliant mechanisms for morphing structural shapes."  
601 *Journal of intelligent material systems and structures*, 14(6), 379–391.

602 Mather, P. T., Luo, X., and Rousseau, I. A. (2009). "Shape memory polymer research." *Annual  
603 Review of Materials Research*, 39, 445–471.

604 Mohaghegh Motlagh, S. A. (2014). "An investigation in structural shape morphing by modulus  
605 variation." Ph.D. thesis, University of Pittsburgh, University of Pittsburgh.

606 Molinari, G., Quack, M., Arrieta, A. F., Morari, M., and Ermanni, P. (2015). "Design, realization  
607 and structural testing of a compliant adaptable wing." *Smart Materials and Structures*, 24(10),  
608 105027.

609 Namgoong, H., Crossley, W., and Lyrintzis, A. (2006). "Morphing airfoil design for  
610 minimum aerodynamic drag and actuation energy including aerodynamic work." *47th  
611 AIAA/ASME/ASCE/AHS/ASC Structures, Structural Dynamics, and Materials Conference 14th  
612 AIAA/ASME/AHS Adaptive Structures Conference 7th*, 2041.

613 Otsuka, K. and Wayman, C. M. (1999). *Shape memory materials*. Cambridge university press.

614 Peraza-Hernandez, E., Hartl, D., and Malak, R. (2013). "Simulation-based design of a self-folding  
615 smart material system." *ASME 2013 International Design Engineering Technical Conferences  
616 and Computers and Information in Engineering Conference*, American Society of Mechanical  
617 Engineers, V06BT07A045–V06BT07A045.

618 Prock, B., Weisshaar, T., and Crossley, W. (2002). "Morphing airfoil shape change optimization with  
619 minimum actuator energy as an objective." *9th AIAA/ISSMO Symposium on Multidisciplinary  
620 Analysis and Optimization*, 5401.



621 Shameri, M., Alghoul, M., Sopian, K., Zain, M. F. M., and Elayeb, O. (2011). “Perspectives of  
622 double skin façade systems in buildings and energy saving.” *Renewable and Sustainable Energy*  
623 *Reviews*, 15(3), 1468–1475.

624 Sun, J., Liu, Y., and Leng, J. (2015). “Mechanical properties of shape memory polymer composites  
625 enhanced by elastic fibers and their application in variable stiffness morphing skins.” *Journal of*  
626 *Intelligent Material Systems and Structures*, 26(15), 2020–2027.

627 Veltkamp, R. C. (2001). “Shape matching: Similarity measures and algorithms.” *Shape Modeling*  
628 *and Applications, SMI 2001 International Conference on.*, IEEE, 188–197.

629 Wang, M., Dutta, D., Kim, K., and Brigham, J. C. (2015). “A computationally efficient approach  
630 for inverse material characterization combining gappy pod with direct inversion.” *Computer*  
631 *Methods in Applied Mechanics and Engineering*, 286, 373–393.

632 Wang, S. and Brigham, J. C. (2012). “A computational framework for the optimal design of mor-  
633 phing processes in locally activated smart material structures.” *Smart Materials and Structures*,  
634 21(10), 105016.

635 Woods, B. K. and Friswell, M. I. (2016). “Multi-objective geometry optimization of the fish bone  
636 active camber morphing airfoil.” *Journal of Intelligent Material Systems and Structures*, 27(6),  
637 808–819.

638 Yu, K., Yin, W., Sun, S., Liu, Y., and Leng, J. (2009). “Design and analysis of morphing wing based  
639 on smp composite.” *Industrial and Commercial Applications of Smart Structures Technologies*  
640 *2009*, Vol. 7290, International Society for Optics and Photonics, 72900S.

641 Zhang, D. and Lu, G. (2004). “Review of shape representation and description techniques.” *Pattern*  
642 *recognition*, 37(1), 1–19.

643 Zupan, R. J., Beblo, R. V., Clifford, D. T., Aggarwal, A., and Brigham, J. C. (2017). “Design  
644 optimization of a self-shading smart material morphing building skin.

645 Zupan, R. J., Clifford, D., Beblo, R., and Brigham, J. (2018). “Numerical investigation of capabili-  
646 ties for dynamic self-shading through shape changing building surface tiles.” *Journal of Facade*  
647 *Design and Engineering*, 6(1).

648  
649  
650  
651  
652  
653

**List of Tables**

1 The design cases considered (in order) to evaluate the computational approach, including whether the target shape was topologically convex and smooth, the degree of spatial variations of the target shape, the mechanisms used for actuating the morphing tile, whether the activation of the morphing tile smart material was localized, and the objective(s) of the optimal design. . . . . 27

Case	Topology	Smoothness	Directions of Spatial Variability	Actuation	Activation	Objective(s)
1	Convex	Smooth and Non-smooth	One	Actuators and Pressure	Full	Shape Difference
2	Non-Convex	Smooth and Non-smooth	One	Actuators and Pressure	Full	Shape Difference
3	Convex and Non-convex	Smooth	One	Actuators and Pressure	Localized	Shape Difference
4	Non-convex	Non-smooth	Two	Pressure	Localized	Shape Difference
5	Convex and Non-convex	Smooth	One	Actuators and Pressure	Localized	Shape Difference and Energy

**TABLE 1.** The design cases considered (in order) to evaluate the computational approach, including whether the target shape was topologically convex and smooth, the degree of spatial variations of the target shape, the mechanisms used for actuating the morphing tile, whether the activation of the morphing tile smart material was localized, and the objective(s) of the optimal design.

654  
655  
656  
657  
658  
659  
660  
661  
662  
663  
664  
665  
666  
667  
668  
669  
670  
671  
672  
673  
674  
675  
676  
677  
678

## List of Figures

1	Concept of a smart material being activated and mechanically actuated. . . . .	31
2	Representation of the distances $D(S_1, S_2)$ and $D(S_2, S_1)$ used in Equation 4 for shapes $S_1$ and $S_2$ . . . . .	32
3	Schematic of the tile concept in which applied pressure ( $P$ ), a series of $n$ discrete actuators at variable locations, and a set of $m$ activation patches (red) at variable locations are used to deform the tile to achieve a given target shape. . . . .	33
4	The two target shapes considered in the convex group. (a) An “overhang” shape (Target Shape 1) and (b) a unidirectional sin-wave (Target Shape 2). . . . .	34
5	(a) Standard Hausdorff distance value and (b) Modified Hausdorff distance for optimal designs using various numbers of actuators for design solutions minimizing with respect to the Standard Hausdorff, Modified Hausdorff, and projection-based distances for Target Shape 1. . . . .	35
6	The morphed tile shape for the “best” design solution, target shape, and actuator placement for the optimization using (a) the Standard Hausdorff distance, (b) the Modified Hausdorff distance, and (c) the projection-based distance for Target Shape 1. . . . .	36
7	(a) Standard Hausdorff distance value and (b) Modified Hausdorff distance for optimal designs using various numbers of actuators for design solutions minimizing with respect to the Standard Hausdorff, Modified Hausdorff, and projection-based distances for Target Shape 2. . . . .	37
8	The morphed tile shape for the “best” design solution, target shape, and actuator placement for the optimization using (a) the Standard Hausdorff distance, (b) the Modified Hausdorff distance, and (c) the projection-based distance for Target Shape 2. . . . .	38
9	The two target shapes considered in the non-convex group. (a) A boxcar function (Target Shape 3) and (b) a distorted sin-wave (Target Shape 4). . . . .	39

679	10	(a) Standard Hausdorff distance value and (b) Modified Hausdorff distance for optimal designs using various numbers of actuators for design solutions minimizing with respect to the Standard Hausdorff and Modified Hausdorff distances for Target Shape 3. . . . .	40
680			
681			
682			
683	11	(a) Standard Hausdorff distance value and (b) Modified Hausdorff distance for optimal designs using various numbers of actuators for design solutions minimizing with respect to the Standard Hausdorff and Modified Hausdorff distances for Target Shape 4. . . . .	41
684			
685			
686			
687	12	The morphed tile shape for the “best” design solution, target shape, and actuator placement for the optimization using (a) the Standard Hausdorff distance and (b) the Modified Hausdorff distance for target shape 3. . . . .	42
688			
689			
690	13	The morphed tile shape for the “best” design solution, target shape, and actuator placement for the optimization using (a) the Standard Hausdorff distance and (b) the Modified Hausdorff distance for Target Shape 4. . . . .	43
691			
692			
693	14	Modified Hausdorff distance values for optimal designs for Target Shape 2 (a) and Target Shape 4 (b) using various numbers of actuators with both localized activation (black) and full activation (gray). . . . .	44
694			
695			
696	15	(a) A cross-sectional view and (b) a top view for the target shape with two directions of spatial variation (a boxcar function), with the hatched section being the raised portion of the target shape. . . . .	45
697			
698			
699	16	The activated (gray) and unactivated (white) portions of the tile for the final design solution for the 3D target shape. . . . .	46
700			
701	17	The morphed tile shape for the design solution and 3D target shape. . . . .	47
702	18	Trade-off between the two objective functions, the Modified Hausdorff distance (x-axis) and morphing energy cost (y-axis) for Target Shape 2 (a) and Target Shape 4 (b). . . . .	48
703			
704			

705 19 The morphed tile shape for the “best” design solution, target shape, and actuator  
706 placement (a) as well as the thermally activated zones (b) for Target Shape 2. . . . 49  
707 20 The morphed tile shape for the “best” design solution, target shape, and actuator  
708 placement (a) as well as the thermally activated zones (b) for Target Shape 4. . . . 50

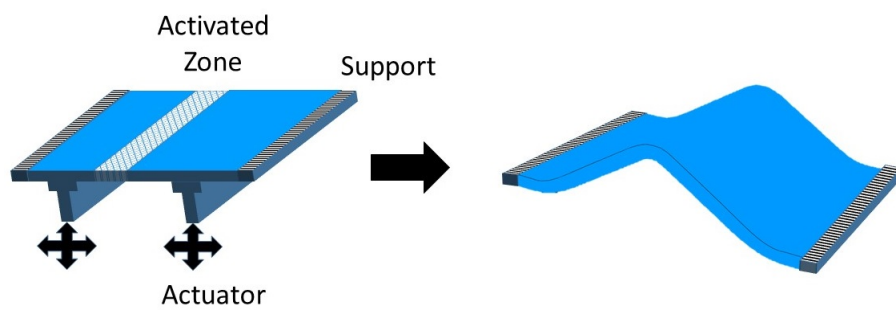


**Fig. 1.** Concept of a smart material being activated and mechanically actuated.

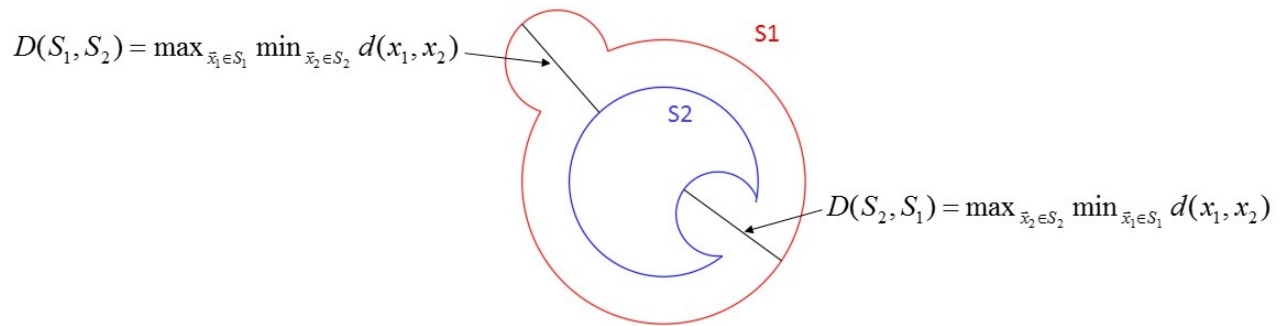


**Fig. 2.** Representation of the distances  $D(S_1, S_2)$  and  $D(S_2, S_1)$  used in Equation 4 for shapes  $S_1$  and  $S_2$



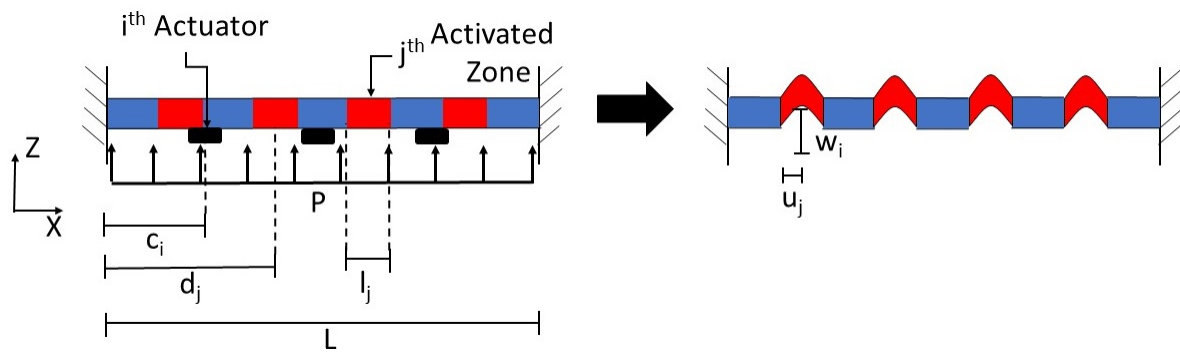


**Fig. 3.** Schematic of the tile concept in which applied pressure ( $P$ ), a series of  $n$  discrete actuators at variable locations, and a set of  $m$  activation patches (red) at variable locations are used to deform the tile to achieve a given target shape.

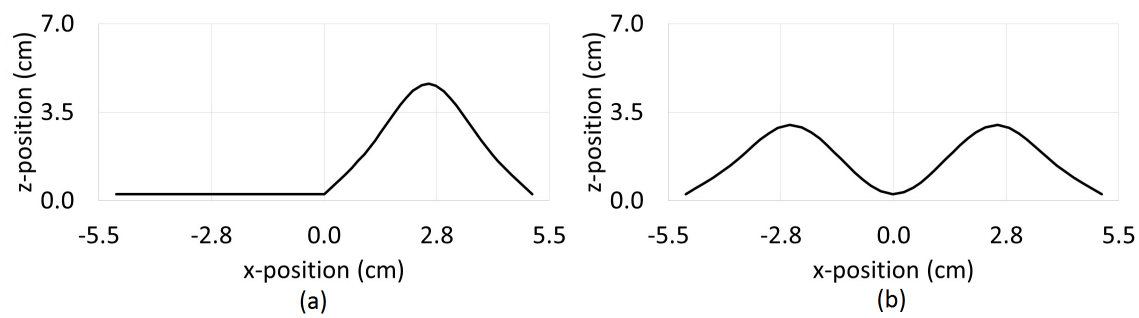


**Fig. 4.** The two target shapes considered in the convex group. (a) An “overhang” shape (Target Shape 1) and (b) a unidirectional sin-wave (Target Shape 2).

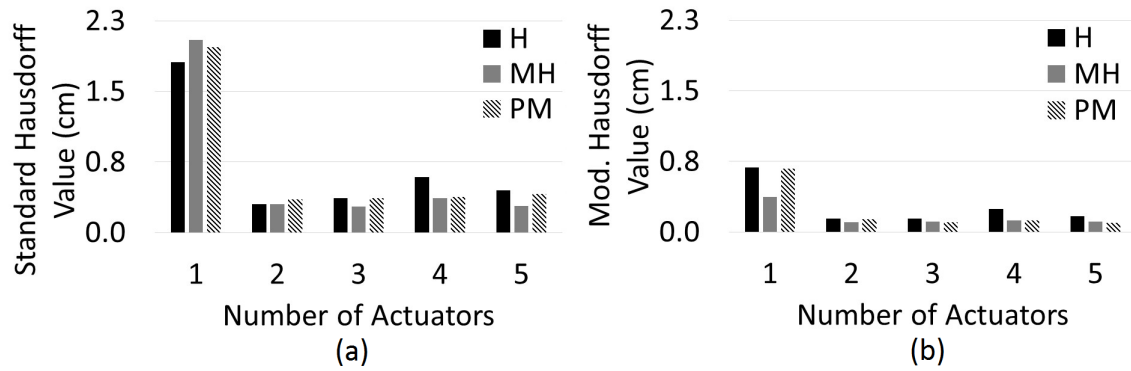


**Fig. 5.** (a) Standard Hausdorff distance value and (b) Modified Hausdorff distance for optimal designs using various numbers of actuators for design solutions minimizing with respect to the Standard Hausdorff, Modified Hausdorff, and projection-based distances for Target Shape 1.

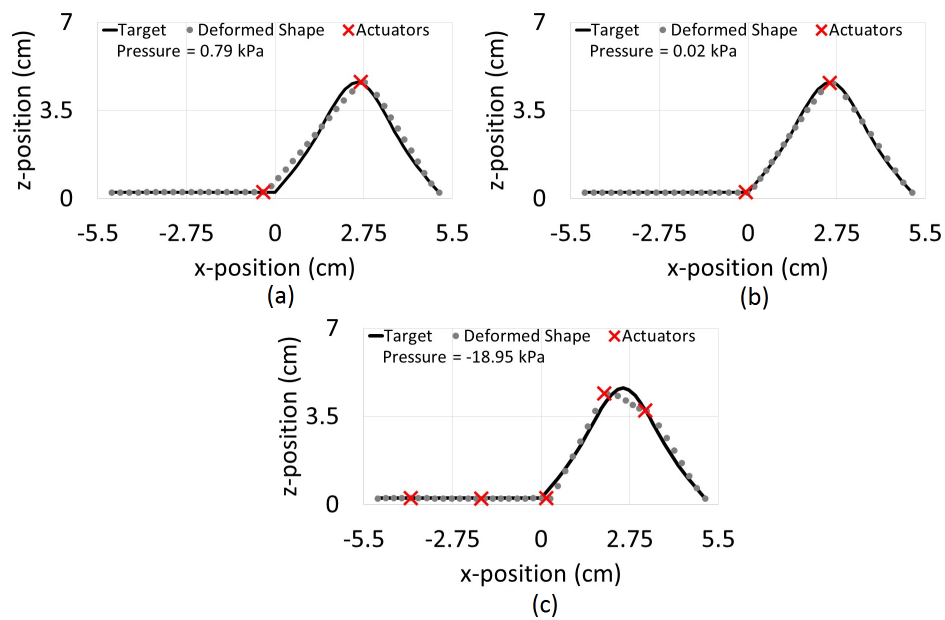


**Fig. 6.** The morphed tile shape for the “best” design solution, target shape, and actuator placement for the optimization using (a) the Standard Hausdorff distance, (b) the Modified Hausdorff distance, and (c) the projection-based distance for Target Shape 1.

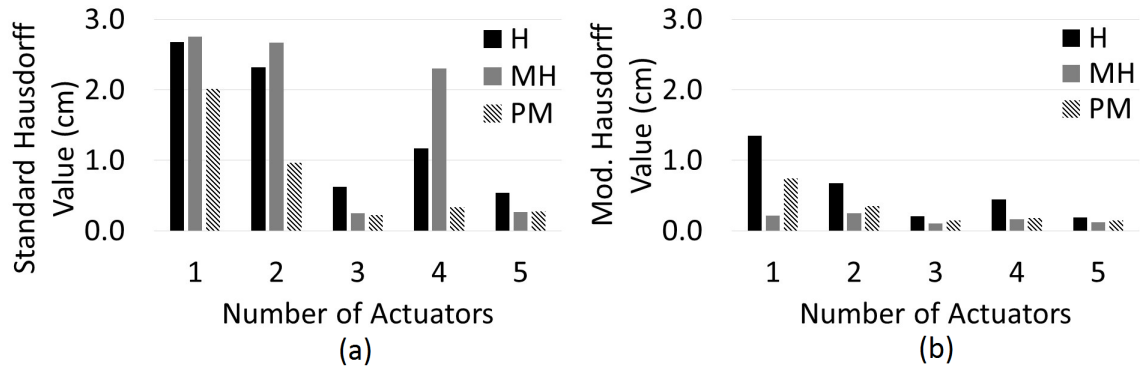


**Fig. 7.** (a) Standard Hausdorff distance value and (b) Modified Hausdorff distance for optimal designs using various numbers of actuators for design solutions minimizing with respect to the Standard Hausdorff, Modified Hausdorff, and projection-based distances for Target Shape 2.

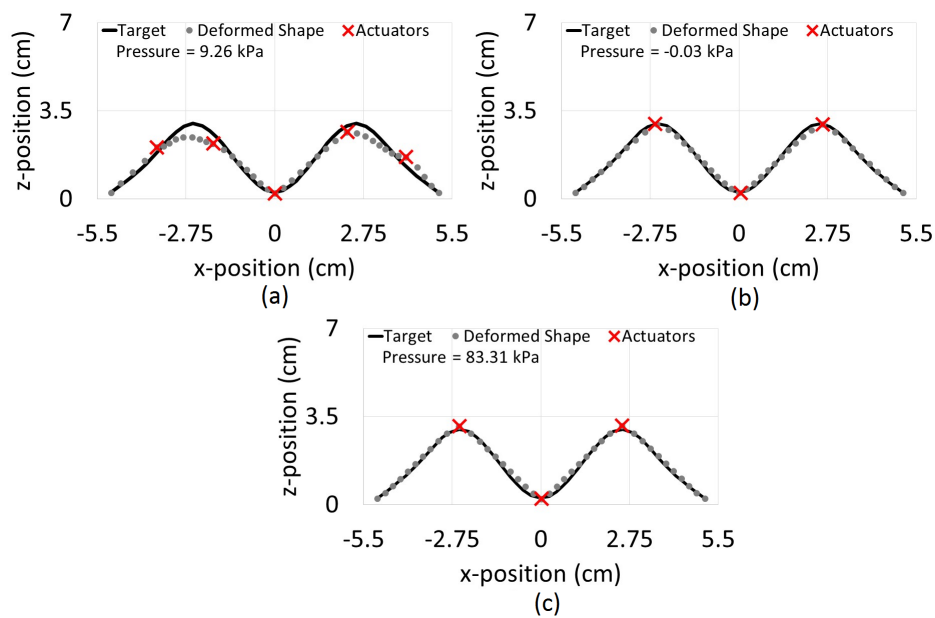


**Fig. 8.** The morphed tile shape for the “best” design solution, target shape, and actuator placement for the optimization using (a) the Standard Hausdorff distance, (b) the Modified Hausdorff distance, and (c) the projection-based distance for Target Shape 2.

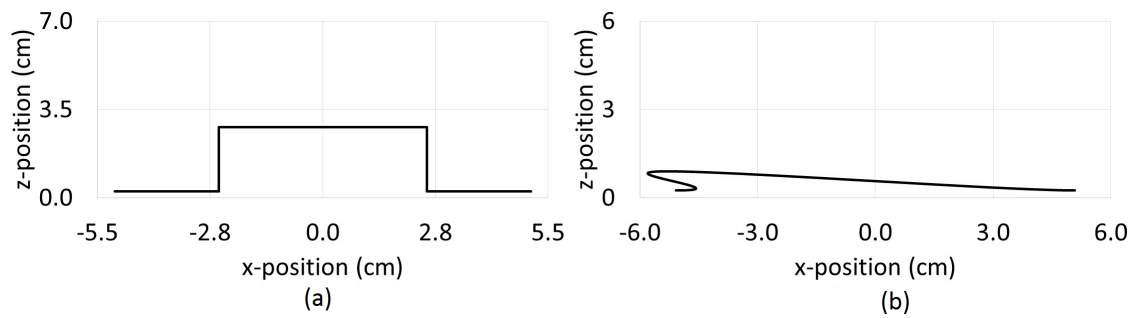


**Fig. 9.** The two target shapes considered in the non-convex group. (a) A boxcar function (Target Shape 3) and (b) a distorted sin-wave (Target Shape 4).

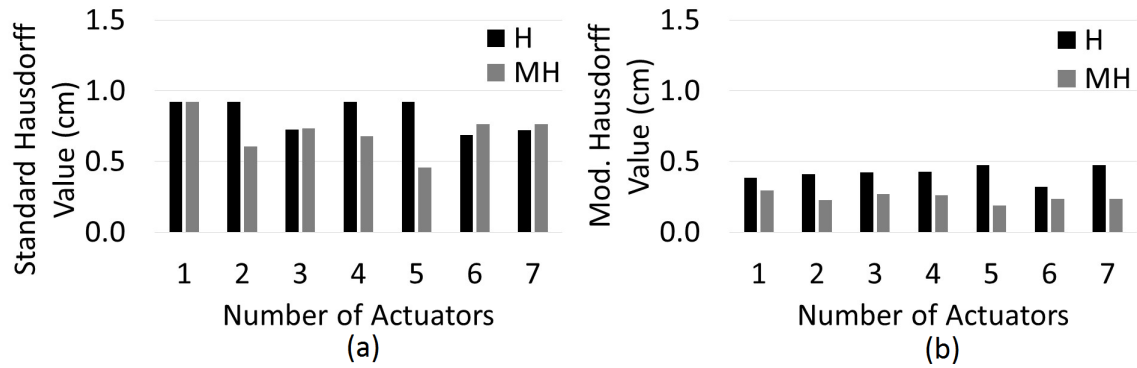


**Fig. 10.** (a) Standard Hausdorff distance value and (b) Modified Hausdorff distance for optimal designs using various numbers of actuators for design solutions minimizing with respect to the Standard Hausdorff and Modified Hausdorff distances for Target Shape 3.



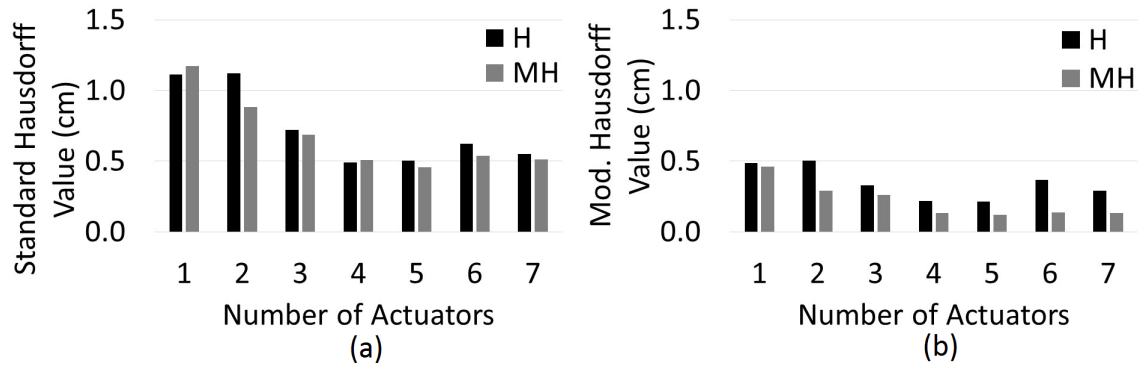


**Fig. 11.** (a) Standard Hausdorff distance value and (b) Modified Hausdorff distance for optimal designs using various numbers of actuators for design solutions minimizing with respect to the Standard Hausdorff and Modified Hausdorff distances for Target Shape 4.

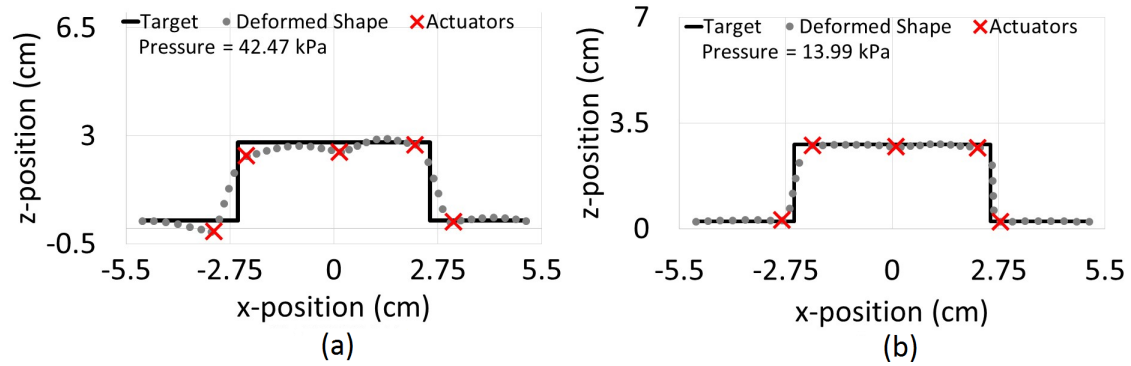


**Fig. 12.** The morphed tile shape for the “best” design solution, target shape, and actuator placement for the optimization using (a) the Standard Hausdorff distance and (b) the Modified Hausdorff distance for target shape 3.

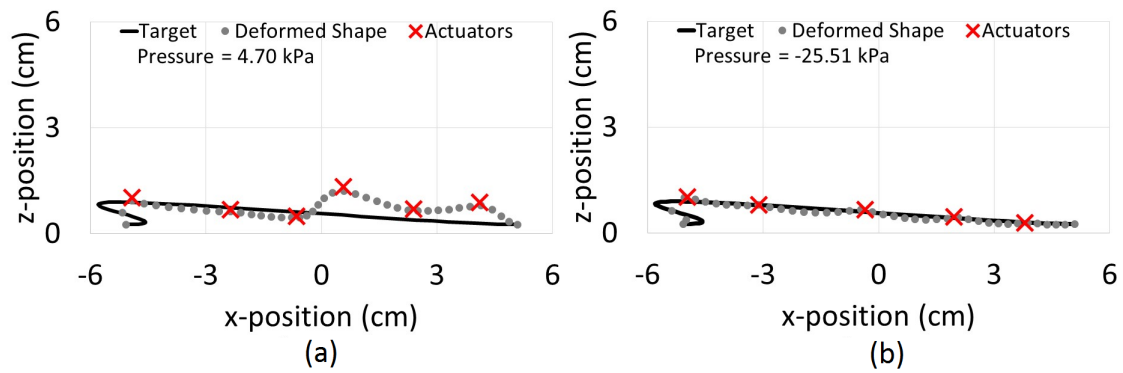


**Fig. 13.** The morphed tile shape for the “best” design solution, target shape, and actuator placement for the optimization using (a) the Standard Hausdorff distance and (b) the Modified Hausdorff distance for Target Shape 4.

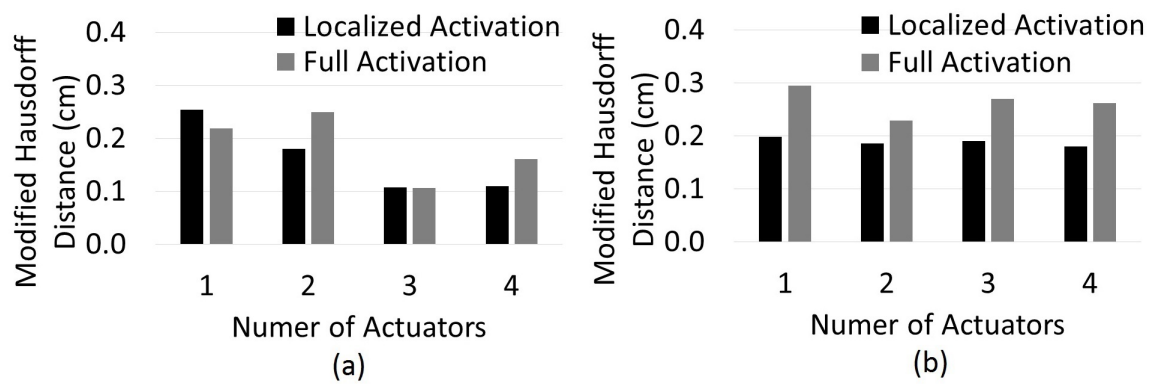


**Fig. 14.** Modified Hausdorff distance values for optimal designs for Target Shape 2 (a) and Target Shape 4 (b) using various numbers of actuators with both localized activation (black) and full activation (gray).

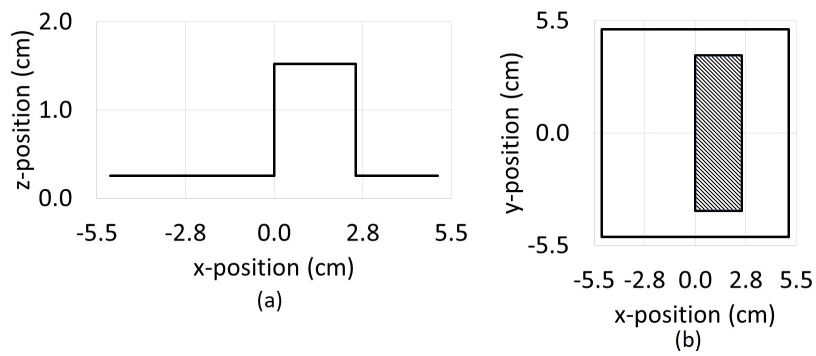


**Fig. 15.** (a) A cross-sectional view and (b) a top view for the target shape with two directions of spatial variation (a boxcar function), with the hatched section being the raised portion of the target shape.

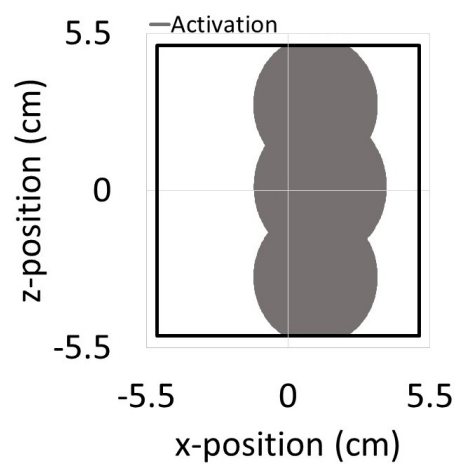


**Fig. 16.** The activated (gray) and unactivated (white) portions of the tile for the final design solution for the 3D target shape.

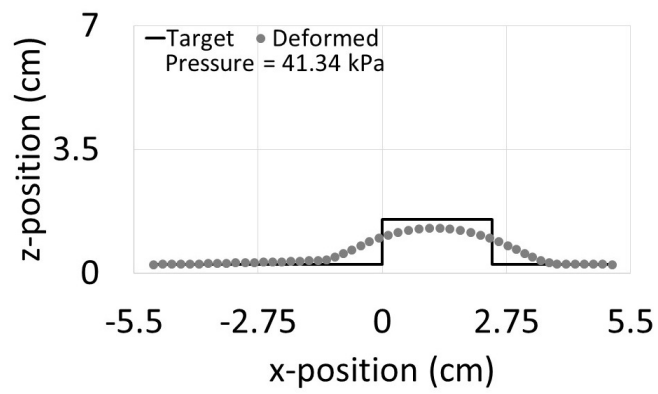


**Fig. 17.** The morphed tile shape for the design solution and 3D target shape.

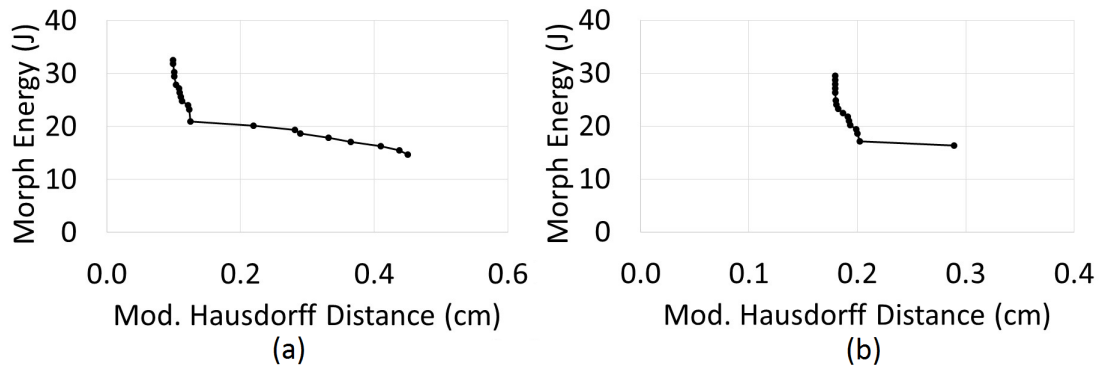


**Fig. 18.** Trade-off between the two objective functions, the Modified Hausdorff distance (x-axis) and morphing energy cost (y-axis) for Target Shape 2 (a) and Target Shape 4 (b).



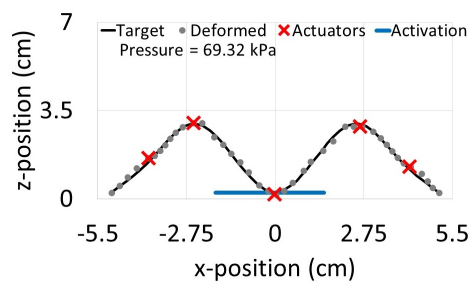


**Fig. 19.** The morphed tile shape for the “best” design solution, target shape, and actuator placement (a) as well as the thermally activated zones (b) for Target Shape 2.

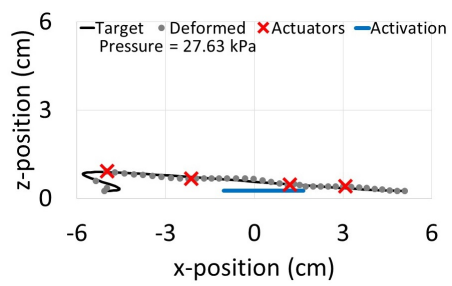


**Fig. 20.** The morphed tile shape for the “best” design solution, target shape, and actuator placement (a) as well as the thermally activated zones (b) for Target Shape 4.